
PTQD: Accurate Post-Training Quantization for Diffusion Models

Yefei He¹ Luping Liu¹ Jing Liu² Weijia Wu¹ Hong Zhou^{1†} Bohan Zhuang^{2†}

¹Zhejiang University, China

²ZIP Lab, Monash University, Australia

Abstract

Diffusion models have recently dominated image synthesis and other related generative tasks. However, the iterative denoising process is expensive in computations at inference time, making diffusion models less practical for low-latency and scalable real-world applications. Post-training quantization of diffusion models can significantly reduce the model size and accelerate the sampling process without requiring any re-training. Nonetheless, applying existing post-training quantization methods directly to low-bit diffusion models can significantly impair the quality of generated samples. Specifically, for each denoising step, quantization noise leads to deviations in the estimated mean and mismatches with the predetermined variance schedule. Moreover, as the sampling process proceeds, the quantization noise may accumulate, resulting in a low signal-to-noise ratio (SNR) during the later denoising steps. To address these challenges, we propose a unified formulation for the quantization noise and diffusion perturbed noise in the quantized denoising process. Specifically, we first disentangle the quantization noise into its correlated and residual uncorrelated parts regarding its full-precision counterpart. The correlated part can be easily corrected by estimating the correlation coefficient. For the uncorrelated part, we subtract the bias from the quantized results to correct the mean deviation and calibrate the denoising variance schedule to absorb the excess variance resulting from quantization. Moreover, we introduce a mixed-precision scheme for selecting the optimal bitwidth for each denoising step, which prioritizes lower bitwidths to expedite early denoising steps, while ensuring that higher bitwidths maintain a high signal-to-noise ratio (SNR) in the later steps. Extensive experiments demonstrate that our method outperforms previous post-training quantized diffusion models in generating high-quality samples, with only a 0.06 increase in FID score compared to full-precision LDM-4 on ImageNet 256×256 , while saving $19.9\times$ bit operations. Code is available at <https://github.com/ziplab/PTQD>.

1 Introduction

Diffusion models have demonstrated remarkable ability in generating high-quality samples in multiple fields [11, 5, 63, 20, 42, 33, 15, 57, 8, 53]. Compared to generative adversarial networks (GANs) [17] and variational autoencoders (VAEs) [30], diffusion models do not face the issue of mode collapse and posterior collapse, thus training is more stable. Nonetheless, the application of diffusion models is limited by two major bottlenecks. Firstly, diffusion models typically require hundreds of denoising steps to generate high-quality samples, making the process significantly slower than that of GANs. To address this, many studies [54, 39, 2, 31, 37] have proposed advanced training-free sampler to reduce the number of denoising iterations. Among them, a recent study DPM-solver [39] curtails the denoising process to ten steps by analytically computing the linear part of the diffusion ordinary

[†]Corresponding author. Email: zhouh@mail.bme.zju.edu.cn, bohan.zhuang@gmail.com



Figure 1: The comparisons of samples generated by Q-Diffusion [34], PTQD and full-precision LDM-4 [49] on CelebA-HQ 256×256 dataset. Here, $WxAy$ indicates the weights are quantized to x -bit while the activations are quantized to y -bit.

differential equations (ODEs). Nevertheless, diffusion models with these fast samplers are not yet ready for real-time applications. For instance, even when executed on a high-performance platform such as the RTX 3090, Stable Diffusion [49] with the DPM-Solver [39] sampler still takes over a second to generate a 512×512 image. Second, the application of diffusion models on various devices is constrained by the massive parameters and computational complexity. To illustrate, executing Stable Diffusion [49] requires 16GB of running memory and GPUs with over 10GB of VRAM, which is infeasible for most consumer-grade PCs, not to mention resource-constrained edge devices.

Model quantization, which employs lower numerical bitwidth to represent weights and activations, has been widely studied to reduce memory footprint and computational complexity. For instance, employing 8-bit models can result in a significant speed-up of $2.2\times$ compared to floating-point models on ARM CPUs [23]. Adopting 4-bit quantization can further deliver a throughput increase of up to 59% compared to 8-bit quantization [3]. To facilitate the quantization process without the need for re-training, post-training quantization (PTQ) has emerged as a widely used technique, which is highly practical and easy to implement. While PTQ on traditional models have been widely studied [44, 35, 22, 36, 62], its application on diffusion models incurs two new challenges at the fundamental level. First, with the noise prediction network quantized, its quantization noise inevitably introduces bias in the estimated mean and brings additional variance that collides with the predetermined variance schedule in each denoising step. Additionally, the quantization noise accumulates as the iterative sampling process progresses, leading to a significant drop in the signal-to-noise ratio (SNR) of the noise prediction network in the later denoising steps. This diminished SNR severely impedes the denoising capability, resulting in a noticeable degradation in the quality of the generated images.

To tackle the aforementioned challenges, we present PTQD, a novel post-training quantization framework for diffusion models. To address the mean deviation and additional variance in each denoising step, we model the quantization noise by disentangling it into its correlated and residual uncorrelated parts regarding its full-precision counterpart, and designs separate correction methods for them. By estimating the correlation coefficient, the correlated part can be easily rectified. For the residual uncorrelated part, we subtract the bias from the estimated mean and propose variance schedule calibration, which absorbs the additional variance into the diffusion perturbed noise. To overcome the issue of low SNR that diminishes denoising capability in later denoising steps, we introduce a step-aware mixed precision scheme, which adaptively allocates different bitwidths for synonymous steps to maintain a high SNR for the denoising process.

In summary, our contributions are as follows:

- We present PTQD, a novel post-training quantization framework for diffusion models, which provides a unified formulation for quantization noise and diffusion perturbed noise.
- We disentangle the quantization noise into correlated and uncorrelated parts regarding its full-precision counterpart. Then we correct the correlated part by estimating the correlation coefficient, and propose variance schedule calibration to rectify the residual uncorrelated part.
- We introduce a step-aware mixed precision scheme, which dynamically selects the appropriate bitwidths for synonymous steps, preserving SNR throughout the denoising process.
- Our extensive experiments demonstrate that our method reaches a new state-of-the-art performance for post-training quantization of diffusion models.

2 Related Work

Efficient diffusion models. While diffusion models can produce high-quality samples, their slow generation speed hinders their large-scale applications in downstream tasks. To explore efficient diffusion models, many methods have been proposed to expedite the sampling process. These methods can be classified into two categories: methods that necessitate re-training and advanced samplers for pre-trained models that do not require training. The first category of methods comprises knowledge distillation [41, 51], diffusion scheme learning [7, 14, 69, 43], noise scale learning [29, 47], and sample trajectory learning [60, 32]. Although these methods can accelerate sampling, re-training a diffusion model can be resource-intensive and time-consuming. On the other hand, the second category of methods designs advanced samplers directly on pre-trained diffusion models, eliminating the need for re-training. The primary methods in this category are implicit sampler [54, 31, 68, 61], analytical trajectory estimation [2, 1], and differential equation (DE) solvers such as customized SDE [55, 25, 28] and ODE [39, 37, 67]. Although these methods can reduce the sampling iterations, the diffusion model’s massive parameters and computational complexity restrict their use to high-performance platforms. Conversely, our proposed low-bit diffusion model can significantly reduce the model’s computational complexity while speeding up the sampling and reducing the demand for hardware computing resources in a training-free manner.

Model quantization. Quantization is a dominant technique to save memory costs and speed up computation. It can be divided into two categories: quantization-aware training (QAT) [16, 38, 24, 70, 66] and post-training quantization (PTQ) [35, 44, 22, 62, 36]. QAT involves simulating quantization during training to achieve good performance with lower precision, but it requires substantial time, computational resources, and access to the original dataset. In contrast, PTQ does not require fine-tuning and only needs a small amount of unlabeled data to calibrate. Recent studies have pushed the limits of PTQ to 4-bit on traditional models by using new rounding strategies [44], layer-wise calibration [22, 58], and second-order statistics [35, 62]. Additionally, mixed precision (MP) [21, 13, 4, 64, 6] allows a part of the model to be represented by lower bitwidths to accelerate inference. Common criteria for determining quantization bitwidths include Hessian spectrum [13, 6] or Pareto frontier [4]. In contrast, we propose a novel mixed-precision scheme for diffusion models that adapts different bitwidths for synonymous denoising steps.

Until now, there have been few studies specifically focusing on quantizing a pre-trained diffusion model without re-training. PTQ4DM [52] is the first attempt to quantize diffusion models to 8-bit, but its experiments are limited to small datasets and low resolution. Q-Diffusion [34] applies advanced PTQ techniques proposed by BRECQ [35] to improve performance and evaluate it on a wider range of datasets. Our paper aims to analyze systematically the quantization effect on diffusion models and establish a unified framework for accurate post-training diffusion quantization.

3 Preliminaries

3.1 Diffusion Models

Diffusion models [54, 19] gradually apply Gaussian noise to real data \mathbf{x}_0 in the forward process and learn a reverse process to denoise and generate high-quality images. For DDPMs [19], the forward process is a Markov chain, which can be formulated as:

$$q(\mathbf{x}_{1:T}|\mathbf{x}_0) = \prod_{t=1}^T q(\mathbf{x}_t|\mathbf{x}_{t-1}), \quad q(\mathbf{x}_t|\mathbf{x}_{t-1}) = \mathcal{N}(\mathbf{x}_t; \sqrt{\alpha_t}\mathbf{x}_{t-1}, \beta_t\mathbf{I}) \quad (1)$$

where α_t, β_t are hyperparameteres and $\beta_t = 1 - \alpha_t$.

In the reverse process, since directly estimating the real distribution of $q(\mathbf{x}_{t-1}|\mathbf{x}_t)$ is intractable, diffusion models approximate it via variational inference by learning a Gaussian distribution $p_\theta(\mathbf{x}_{t-1}|\mathbf{x}_t) = \mathcal{N}(\mathbf{x}_{t-1}; \boldsymbol{\mu}_\theta(\mathbf{x}_t, t), \boldsymbol{\Sigma}_\theta(\mathbf{x}_t, t))$ and reparameterize its mean by a noise prediction network $\boldsymbol{\epsilon}_\theta(\mathbf{x}_t, t)$:

$$\boldsymbol{\mu}_\theta(\mathbf{x}_t, t) = \frac{1}{\sqrt{\alpha_t}} \left(\mathbf{x}_t - \frac{\beta_t}{\sqrt{1 - \bar{\alpha}_t}} \boldsymbol{\epsilon}_\theta(\mathbf{x}_t, t) \right) \quad (2)$$

where $\bar{\alpha}_t = \prod_{s=1}^t \alpha_s$. The variance $\Sigma_\theta(\mathbf{x}_t, t)$ can either be reparameterized or fixed to a constant schedule σ_t . When it uses a constant schedule, the sampling of \mathbf{x}_{t-1} can be formulated as:

$$\mathbf{x}_{t-1} = \frac{1}{\sqrt{\alpha_t}} \left(\mathbf{x}_t - \frac{\beta_t}{\sqrt{1 - \bar{\alpha}_t}} \boldsymbol{\epsilon}_\theta(\mathbf{x}_t, t) \right) + \sigma_t \mathbf{z}, \text{ where } \mathbf{z} \sim \mathcal{N}(\mathbf{0}, \mathbf{I}). \quad (3)$$

Our method focuses on post-training quantization of diffusion models without the need of training. Instead, we use pre-trained diffusion models and inherit their hyperparameters and variance schedules for inference. Although the derivations presented in this paper are based on DDPM, they can be readily extended to other fast sampling methods, such as DDIM [54]. Additional information can be found in the supplementary material.

3.2 Model Quantization

We use uniform quantization in our study and all the experiments. For uniform quantization, given a floating-point vector \mathbf{x} , the target bitwidth b , the quantization process can be defined as:

$$\hat{\mathbf{x}} = \Delta \cdot \left(\text{clip}(\lfloor \frac{\mathbf{x}}{\Delta} \rfloor + Z, 0, 2^b - 1) - Z \right), \quad (4)$$

where $\lfloor \cdot \rfloor$ is the round operation, $\Delta = \frac{\max(\mathbf{x}) - \min(\mathbf{x})}{2^b - 1}$ and $Z = -\lfloor \frac{\min(\mathbf{x})}{\Delta} \rfloor$.

To ensure clarity and consistency, we introduce notation to define the variables used in the paper. Let X be a tensor (weights or activations) in the full-precision model, the result after normalization layers is denoted as \bar{X} . The corresponding tensor of the quantized model is represented as \hat{X} . The quantization noise is depicted by Δ_X , which is the difference between \hat{X} and X .

4 Method

Model quantization discretizes the weights and activations, which will inevitably introduce quantization noise into the result. As per Eq. (3), during the reverse process of the quantized diffusion model, the sampling of \mathbf{x}_{t-1} can be expressed as:

$$\begin{aligned} \mathbf{x}_{t-1} &= \frac{1}{\sqrt{\alpha_t}} \left(\mathbf{x}_t - \frac{\beta_t}{\sqrt{1 - \bar{\alpha}_t}} \hat{\boldsymbol{\epsilon}}_\theta(\mathbf{x}_t, t) \right) + \sigma_t \mathbf{z} \\ &= \frac{1}{\sqrt{\alpha_t}} \left(\mathbf{x}_t - \frac{\beta_t}{\sqrt{1 - \bar{\alpha}_t}} (\boldsymbol{\epsilon}_\theta(\mathbf{x}_t, t) + \Delta_{\boldsymbol{\epsilon}_\theta(\mathbf{x}_t, t)}) \right) + \sigma_t \mathbf{z}. \end{aligned} \quad (5)$$

Here, $\hat{\boldsymbol{\epsilon}}_\theta(\mathbf{x}_t, t)$ is the output of the quantized noise prediction network and $\Delta_{\boldsymbol{\epsilon}_\theta(\mathbf{x}_t, t)}$ refers to the quantization noise. The additional quantization noise will inevitably alter the mean and variance of \mathbf{x}_{t-1} , decreasing the signal-to-noise ratio (SNR) and adversely affecting the quality of the generated samples. Therefore, to mitigate the impact of quantization, it is necessary to correct the mean and variance to restore the SNR at each step of the reverse process.

4.1 Correlation Disentanglement

We begin by making an assumption that a correlation exists between the quantization noise and the result of the full-precision noise prediction network. While other factors, such as nonlinear operations, may contribute to this correlation, *Proposition 1* demonstrates that normalization layers are responsible for a part of it.

Proposition 1. *Given Y and \hat{Y} as inputs to a normalization layer in a full-precision model and its quantized version, where the quantization noise $\Delta_Y = \hat{Y} - Y$ is initially uncorrelated with Y , a correlation between the quantization noise and the output of the full-precision model after the normalization layer will exist.*

The proof is based on the fact that the mean and variance of \hat{Y} will differ from that of Y (depending on the specific quantization scheme). Therefore, the quantization noise after normalization layer can be expressed as :

$$\Delta_{\bar{Y}} = \frac{\hat{Y} - \mu_{\hat{Y}}}{\sigma_{\hat{Y}}} - \frac{Y - \mu_Y}{\sigma_Y} = \frac{\sigma_Y \Delta_Y - (\sigma_{\hat{Y}} - \sigma_Y)Y + \sigma_{\hat{Y}} \mu_Y - \sigma_Y \mu_{\hat{Y}}}{\sigma_{\hat{Y}} \sigma_Y}. \quad (6)$$

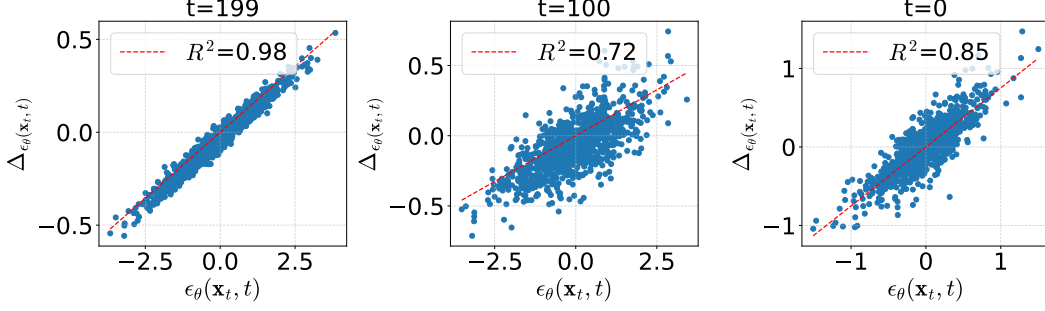


Figure 2: The correlation between the quantization noise (Y-axis) and the output of the full-precision noise prediction network (X-axis). Each data point on the plot corresponds to specific entries within these vectors. Data were collected by generating samples with 4-bit LDM-8 [49] for 200 steps on LSUN-Churches [65].

Here, we omit the affine transform parameters in normalization layers for simplicity. It can be observed from Eq. (6) that the second term in the numerator is related to Y , while the other three terms are uncorrelated. Therefore, after normalization layers, the quantization noise $\Delta_{\mathcal{Y}}$ will be correlated with Y .

The empirical observation illustrated in Figure 2 confirms a strong correlation between the quantization noise and the output of the full-precision noise prediction network, which further verifies our assumption. Based on the assumption and observation, the quantization noise of the quantized noise prediction network can be disentangled into two parts:

$$\Delta_{\epsilon_{\theta}(\mathbf{x}_t, t)} = k\epsilon_{\theta}(\mathbf{x}_t, t) + \Delta'_{\epsilon_{\theta}(\mathbf{x}_t, t)}. \quad (7)$$

The first part, denoted by $k\epsilon_{\theta}(\mathbf{x}_t, t)$, is linearly related to $\epsilon_{\theta}(\mathbf{x}_t, t)$. The second part, expressed by $\Delta'_{\epsilon_{\theta}(\mathbf{x}_t, t)}$, represents the residual component of the quantization noise, and is assumed to be uncorrelated with $\epsilon_{\theta}(\mathbf{x}_t, t)$. Here, k is the correlation coefficient, which can be estimated by applying linear regression on the quantization noise $\Delta_{\epsilon_{\theta}(\mathbf{x}_t, t)}$ and the original value $\epsilon_{\theta}(\mathbf{x}_t, t)$. Details can be found in Section 5.1.

With the disentanglement presented in Eq. (7), the sampling of \mathbf{x}_{t-1} can be further expressed as:

$$\begin{aligned} \mathbf{x}_{t-1} &= \frac{1}{\sqrt{\alpha_t}} \left(\mathbf{x}_t - \frac{\beta_t}{\sqrt{1-\alpha_t}} (\epsilon_{\theta}(\mathbf{x}_t, t) + \Delta_{\epsilon_{\theta}(\mathbf{x}_t, t)}) \right) + \sigma_t \mathbf{z} \\ &= \frac{1}{\sqrt{\alpha_t}} \left(\mathbf{x}_t - \frac{\beta_t}{\sqrt{1-\alpha_t}} \left((1+k)\epsilon_{\theta}(\mathbf{x}_t, t) + \Delta'_{\epsilon_{\theta}(\mathbf{x}_t, t)} \right) \right) + \sigma_t \mathbf{z}. \end{aligned} \quad (8)$$

Consequently, the bias and additional variance arise from both the correlated and uncorrelated parts of quantization noise. In the following section, we will provide a detailed explanation of how these two parts of quantization noise can be separately corrected.

4.2 Quantization Noise Correction

4.2.1 Correlated Noise Correction

Based on Eq. (8), the correlated part of the quantization noise can be rectified by dividing the output of the quantized noise prediction network $\hat{\epsilon}_{\theta}(\mathbf{x}_t, t)$ by $1+k$, resulting in:

$$\mathbf{x}_{t-1} = \frac{1}{\sqrt{\alpha_t}} \left(\mathbf{x}_t - \frac{\beta_t}{\sqrt{1-\alpha_t}} \epsilon_{\theta}(\mathbf{x}_t, t) \right) + \sigma_t \mathbf{z} - \frac{\beta_t}{\sqrt{\alpha_t} \sqrt{1-\alpha_t} (1+k)} \Delta'_{\epsilon_{\theta}(\mathbf{x}_t, t)}. \quad (9)$$

Consequently, only the uncorrelated quantization noise remains. Moreover, for values of $k \geq 0$, it can be deduced that the mean and variance of the uncorrelated quantization noise are diminished by $\frac{1}{1+k}$. In practice, we enforce the non-negativity of k , and reset it to zero if it is negative. In the following, we will explain how to handle the uncorrelated quantization noise that persists in Eq. (9).

4.2.2 Uncorrelated Noise Correction

The presence of uncorrelated quantization noise introduces additional variance at each step, resulting in a total variance that exceeds the scheduled value σ_t^2 . To address this, we propose to calibrate the variance schedule for quantized diffusion models, which is denoted as $\sigma_t'^2$ and smaller than the original schedule σ_t^2 . To estimate $\sigma_t'^2$, we further make an assumption and model the uncorrelated quantization noise as a Gaussian distribution with a mean of μ_q and a variance of σ_q^2 :

$$\Delta'_{\epsilon_\theta(\mathbf{x}_t, t)} \sim \mathcal{N}(\mu_q, \sigma_q). \quad (10)$$

To verify this assumption, we conduct statistical tests (refer to the supplementary material) and present the distribution of the uncorrelated quantization noise in Figure 3. The values of mean and variance can be estimated by generating samples with both quantized and full-precision diffusion models and collecting the statistics of the uncorrelated quantization noise. Following prior work [45], the mean deviation can be rectified through Bias Correction (BC), where we collect the channel-wise means of uncorrelated quantization noise and subtract them from the output of quantized noise prediction network. For the variance of the uncorrelated quantization noise, we propose Variance Schedule Calibration (VSC), where the uncorrelated quantization noise can be absorbed into Gaussian diffusion noise with the above assumption. By substituting the calibrated variance schedule $\sigma_t'^2$ into Eq. (9) while keeping the variance of each step unaltered, we can solve for the optimal variance schedule using the following approach:

$$\sigma_t'^2 + \frac{\beta_t^2}{\alpha_t(1-\bar{\alpha}_t)(1+k)^2} \sigma_q^2 = \sigma_t^2, \quad (11)$$

$$\sigma_t'^2 = \begin{cases} \sigma_t^2 - \frac{\beta_t^2}{\alpha_t(1-\bar{\alpha}_t)(1+k)^2} \sigma_q^2, & \text{if } \sigma_t^2 \geq \frac{\beta_t^2}{\alpha_t(1-\bar{\alpha}_t)(1+k)^2} \sigma_q^2 \\ 0, & \text{otherwise.} \end{cases} \quad (12)$$

It can be observed that if the additional variance of quantization noise is smaller than the noise hyperparameter σ_t^2 , the increase in variance caused by quantization can be eliminated. According to Eq. (12), the coefficient for the variance of the quantization noise can be calculated as $\frac{\beta_t^2}{\alpha_t(1-\bar{\alpha}_t)(1+k)^2}$, which is generally small enough to ensure that the quantization noise can be fully absorbed, except for cases of deterministic sampling where σ_t is zero. In this case, there is no analytical solution for $\sigma_t'^2$, and we use the optimal solution that is $\sigma_t'^2 = 0$. Overall, the process quantization noise correction is summarized in Algorithm 1.

Algorithm 1: Quantization noise correction.

Statistics collection before sampling:

- 1) Quantize diffusion models with BRECQ [35] (or other PTQ methods);
- 2) Generate samples with both quantized and FP models and collect quantization noise;
- 3) Calculate the correlated coefficient k based on Eq. (7), and the mean and variance of the uncorrelated quantization noise as per Eq. (10);

Noise correction for each sampling step:

- 4) Correct the correlated part of the quantization noise by dividing the output of the noise prediction network by $1+k$;
 - 5) Calibrate the variance schedule by Eq. (12) and subtract the channel-wise biases from the output of the quantized noise prediction network.
-

Although the proposed method can correct the mean deviation and the numerical value of the variance for each step, generating satisfactory samples with low-bit diffusion models remains challenging due to the low signal-to-noise ratio (SNR) of the quantized noise prediction network. In the next section, we will analyze this issue in detail.

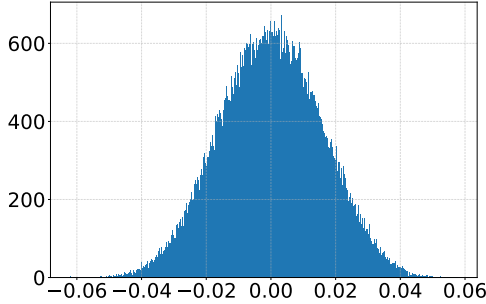


Figure 3: The distribution of uncorrelated quantization noise collected from W4A8 LDM-4 on LSUN-Bedrooms 256×256 dataset, where the x-axis represents the range of values and the y-axis is the frequency of values.

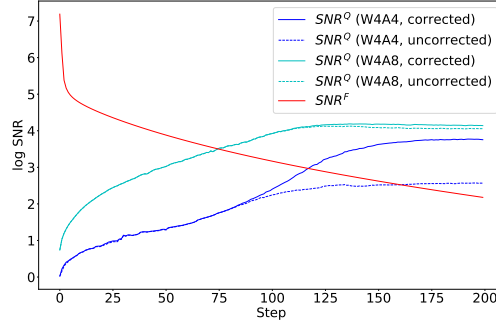


Figure 4: Comparison of the signal-to-noise-ratio (SNR) in each step of LDM-4 on LSUN-Bedrooms across various bitwidths.

4.3 Step-aware Mixed Precision

Given the output of the full-precision noise prediction network $\epsilon_\theta(\mathbf{x}_t, t)$ and corresponding quantization noise $\Delta_{\epsilon_\theta(\mathbf{x}_t, t)}$, we define the SNR^Q of quantized noise prediction network by:

$$\text{SNR}^Q(t) = \frac{\|\epsilon_\theta(\mathbf{x}_t, t)\|_2}{\|\Delta_{\epsilon_\theta(\mathbf{x}_t, t)}\|_2}. \quad (13)$$

Figure 4 depicts the SNR^Q with various bitwidths and correction methods. The figure reveals several insights: 1) SNR^Q drops drastically as step t decreases; 2) models with higher bitwidth exhibit larger SNR^Q ; 3) the proposed correction methods yield clear SNR^Q improvements, especially for large steps. The first observation highlights the challenge of generating high-quality samples using low-bit diffusion models. In particular, as t approaches zero, the SNR^Q of W4A4 diffusion models diminishes and approaches unity, implying that the magnitude of quantization noise is even comparable to the original result of the noise prediction network. To enable low-bit diffusion models while maintaining good generation performance, we propose a novel approach called Step-aware Mixed Precision, which involves setting different bitwidths for synonymous steps to keep SNR^Q within a reasonable range across all steps.

Specifically, the bitwidth of weights is fixed and shared across different denoising steps, which eliminates the need to store and reload multiple model state files during the sampling process. As a result, we only adjust the bitwidth of activations. Formally, we predefine a set of bitwidths $B = \{b_1, b_2, \dots, b_n\}$ for activations and evaluate the SNR^Q under each bitwidth. To establish a benchmark for SNR^Q , we follow prior studies [39, 29] and introduce SNR^F based on the forward process, which denotes the degree of data noise at each step:

$$\text{SNR}^F(t) = \alpha_t^2 / \sigma_t^2. \quad (14)$$

Figure 4 illustrates $\text{SNR}^F(t)$, which decreases strictly with respect to steps t . To determine the optimal bitwidth for each step t , we compare the SNR^Q of each bitwidth with SNR^F , and select the minimum bitwidth b_{\min} that satisfies:

$$\text{SNR}_{b_{\min}}^Q(t) > \text{SNR}^F(t). \quad (15)$$

If none of the bitwidths satisfies this condition, we utilize the maximum bitwidth in B to achieve a higher SNR. In practice, models with different bitwidths are calibrated separately, with the calibration set collected from the corresponding steps.

5 Experiments

5.1 Implementation Details

Datasets and quantization settings. We conduct image synthesis experiments using latent diffusion models (LDM) [49] on three standard benchmarks: ImageNet[10], LSUN-Bedrooms, and LSUN-Churches [65], each with a resolution of 256×256 . All experimental configurations, including the number of steps, variance schedule (denoted by *eta* in the following), and classifier-free guidance scale, follow the official implementation [49]. For low-bit quantization, we use the PTQ method proposed in BRECQ [35] and AdaRound [44], which is congruent with Q-Diffusion [34]. For 8-bit quantization on ImageNet, we only use a naive PTQ method proposed by TensorRT [48], which is simple and fast. The input and output layers in the model are fixed to 8-bit, while all other convolutional and linear layers are quantized to the target bitwidth. In mixed precision experiments, we fix the weights to 4-bit and use Eq. (15) to determine the bitwidth of activations over uncorrected quantized diffusion models with a bitwidth set of $\{4, 8\}$. Details of bitwidth allocation can be found in the supplementary material.

Evaluation metrics. For each experiment, we report the widely adopted Frechet Inception Distance (FID) [18] and sFID [46] to evaluate the performance. For ImageNet experiments, we additionally report Inception Score (IS) [50] for reference. To ensure consistency in the reported outcomes, including those of the baseline methods, all results are obtained by our implementation. We sample 50,000 images and evaluate them with ADM’s TensorFlow evaluation suite [11]. To quantify the computational efficiency, we measure Bit Operations (BOPs) for a single forward pass of the diffusion model using the equation $BOPs = MACs \cdot b_w \cdot b_a$, where MACs denotes Multiply-And-Accumulate operations, and b_w and b_a represent the bitwidth of weights and activations, respectively, following [59].

Statistics collection. Before implementing our method, three statistics need to be collected: the correlation coefficient, denoted as k in Eq. (7), and the mean and variance of the uncorrelated quantization noise, as depicted in Eq. (10). To obtain these statistics, we generate 1024 samples using both quantized and full-precision diffusion models, store the quantization noise at each step, and then calculate the required statistics.

5.2 Ablation Study

As shown in Table 1, we conduct ablation experiments on ImageNet 256×256 dataset over LDM-4 model, to demonstrate the effectiveness of the proposed techniques. These techniques include Correlated Noise Correction (CNC) for addressing the correlated quantization noise, as well as Bias Correction (BC) and Variance Schedule Calibration (VSC) for correcting the residual uncorrelated quantization noise. By employing Correlated Noise Correction, we achieved a 0.48 reduction in FID and a 6.55 decrease in sFID. The considerable reduction in sFID suggests that the generated images possess more intricate spatial details than those generated using the baseline method, and that the correlated portions significantly contribute to the quantization noise. With the proposed Variance Schedule Calibration, the additional variance of uncorrelated quantization noise can be absorbed, achieving a reduction of 0.2 in FID and 0.11 in sFID. By further introducing Bias Correction that effectively corrects the mean deviation caused by quantization noise, our proposed PTQD achieved an FID of 6.44 and an sFID of 8.43, with only a 1.33 increase in sFID under the W4A4/W4A8 mixed precision setting. These results demonstrate the efficacy of the proposed techniques in achieving accurate post-training quantization of diffusion models.

Additional ablation experiments can be found in the supplementary material.

5.3 Main Results

5.3.1 Class-conditional Generation

In this section, we evaluate the performance of class-conditional image generation on 256×256 ImageNet dataset, as presented in Table 2. By utilizing the Naive PTQ method [48] and quantizing to 8-bit, diffusion models can achieve a notable $12.39\times$ reduction in bit operations, while experiencing minimal increases in FID/sFID. With the aggressive W4A8 bitwidth setting, our method effectively narrows the FID gap to a mere 0.06 with 250 generation steps. In this setting, the model size is

Table 1: The effect of different components proposed in the paper. Here, MP denotes the proposed step-aware mixed precision scheme.

Models	Method	Bitwidth (W/A)	FID↓	sFID↓
LDM-4 (steps = 250 eta = 1.0 scale = 1.5)	Q-Diffusion	MP	9.97	18.23
	+ CNC	MP	9.49	11.68
	+ CNC + VSC	MP	9.29	11.57
	PTQD (CNC + VSC + BC)	MP	6.44	8.43
	FP	32/32	5.05	7.10

compressed by $6.83\times$ and the bit operations can be reduced by a remarkable $19.96\times$. In experiments utilizing mixed precision with W4A4 and W4A8 bitwidths, previous methods encounter difficulties in mitigating substantial quantization noises caused by low-bit quantization. For instance, in the first set of experiments with a 20-step generation process, Q-Diffusion [34] obtains FID and sFID scores as high as 116.61 and 172.99, respectively, indicating difficulties in handling low-bit diffusion models with fewer generation steps. While our method cannot calibrate the variance schedule due to a zero value for the hyperparameter η , it still achieves an exceptionally low FID score of 7.75, demonstrating effective rectification of the correlated quantization noise and mean deviation. The second set of mixed precision experiments also yielded similar results, with our method reducing FID and sFID scores by 3.53 and 9.80, respectively.

Table 2: Performance comparisons of class-conditional image generation on ImageNet 256×256 .

Model	Method	Bitwidth (W/A)	Model Size (MB)	BOPs (T)	BOP comp. ratio	IS↑	FID↓	sFID↓
LDM-4 (steps = 20 eta = 0.0 scale = 3.0)	FP	32/32	1603.35	102.21	-	225.16	12.45	7.85
	Naive PTQ	8/8	430.06	8.25	$12.39\times$	152.91	12.14	8.43
	Ours	8/8	430.06	8.25	$12.39\times$	153.92	11.94	8.03
	Q-Diffusion	4/8	234.51	5.12	$19.96\times$	212.52	10.63	14.80
	Ours	4/8	234.51	5.12	$19.96\times$	214.73	10.40	12.68
	Q-Diffusion	MP	234.51	4.73	$21.61\times$	7.86	116.61	172.99
	Ours	MP	234.51	4.73	$21.61\times$	175.19	7.75	18.78
	FP	32/32	1603.35	102.21	-	185.04	5.05	7.10
LDM-4 (steps = 250 eta = 1.0 scale = 1.5)	Naive PTQ	8/8	430.06	8.25	$12.39\times$	180.56	4.06	5.91
	Ours	8/8	430.06	8.25	$12.39\times$	180.83	4.02	5.81
	Q-Diffusion	4/8	234.51	5.12	$19.96\times$	148.74	5.37	9.56
	Ours	4/8	234.51	5.12	$19.96\times$	149.74	5.11	8.49
	Q-Diffusion	MP	234.51	4.81	$21.25\times$	121.10	9.97	18.23
	Ours	MP	234.51	4.81	$21.25\times$	126.26	6.44	8.43

5.4 Unconditional Generation

In this section, we present a comprehensive evaluation of our approach on LSUN-Bedrooms and LSUN-Churches [65] datasets for unconditional image generation. As shown in Table 3, our method consistently narrows the performance gap between quantized and full-precision diffusion models. Notably, our proposed method allows for compression of diffusion models to 8-bit with minimal performance degradation, resulting in a mere 0.1 increase in FID on the LSUN-Churches dataset. With the W4A8 bitwidth setting, our method reduces FID and sFID by notably 0.78 and 3.61 compared with Q-Diffusion [34] on LSUN-Bedrooms. Furthermore, Q-Diffusion fails to effectively denoise samples under the mixed precision setting on LSUN-Churches due to its low SNR. In this case, the hyperparameter η is set to zero, which prevents the use of Variance Schedule Calibration. Despite relying solely on Correlated Noise Correction and Bias Correction, our approach remarkably enhances the quality of the generated images, as demonstrated by a substantial reduction in the FID score from 218.59 to 17.99. This notable improvement highlights the significant impact of the correlated part of quantization noise on the overall image quality, which can be effectively rectified by our method.

Additional evaluation results on CelebA-HQ dataset can be found in the supplementary material.

Table 3: Performance comparisons of unconditional image generation.

LSUN-Bedrooms 256×256 LDM-4 (steps = 200, eta = 1.0)				LSUN-Churches 256×256 LDM-8 (steps = 200, eta = 0.0)			
Method	Bitwidth (W/A)	FID↓	sFID↓	Method	Bitwidth (W/A)	FID↓	sFID↓
Full precision	32/32	3.00	7.13	Full precision	32/32	6.30	18.24
Q-Diffusion	8/8	3.80	9.95	Q-Diffusion	8/8	6.94	18.93
Ours	8/8	3.75	9.89	Ours	8/8	6.40	18.34
Q-Diffusion	4/8	6.72	18.80	Q-Diffusion	4/8	7.80	19.97
Ours	4/8	5.94	15.16	Ours	4/8	7.33	19.40
Q-Diffusion	MP	5.75	12.79	Q-Diffusion	MP	218.59	312.86
Ours	MP	5.49	12.04	Ours	MP	17.99	37.34

5.5 Deployment Efficiency

We have measured the latency of matrix multiplication and convolution operations in quantized and full-precision diffusion models using an RTX3090 GPU, as shown in Table 4. Both floating-point and quantized operations are implemented with CUTLASS [27]. When both weights and activations are quantized to 8-bit, we observe a $2.03\times$ reduction in latency compared to its full-precision counterpart over LDM-4. Moreover, when weights and activations are quantized to 4-bit, the speedup further increases to $3.34\times$. The mixed-precision settings explored in our experiments strike a good balance between latency and model performance.

Table 4: Comparisons of time cost across various bitwidth configurations on ImageNet 256×256 . Due to the current lack of a fast implementation for W4A8, we implement MP scheme with W8A8 and W4A4 kernels.

Model	Bitwidth (W/A)	Model Size (MB)	FID↓	sFID↓	Time (s)
LDM-4	32/32	1603.35	5.05	7.10	5.46
(steps=250	8/8	430.06	4.02	5.81	2.68
eta=1.0	MP	234.51	6.44	8.43	2.45
scale=1.5)	4/4	234.51	-	-	1.63

6 Conclusion and Future Work

In this paper, we have proposed PTQD, a novel post-training quantization framework for diffusion models that unifies the formulation of quantization noise and diffusion perturbed noise. To start with, we have disentangled the quantization noise into correlated and residual uncorrelated parts relative to its full-precision counterpart. To reduce mean deviations and additional variance in each step, the correlated part can be easily corrected by estimating the correlation coefficient. For the uncorrelated part, we have proposed Variance Schedule Calibration to absorb its additional variance and Bias Correction to correct the mean deviations. Moreover, we have introduced Step-aware Mixed Precision to adaptively select the optimal bitwidth for each denoising step. By incorporating these techniques, our PTQD has achieved significant performance improvement over existing state-of-the-art post-training quantized diffusion models, with only a 0.06 FID increase compared to the full-precision LDM-4 on ImageNet 256×256 while saving $19.9\times$ bit-operations. In the future, we can further quantize other components within diffusion models, such as the text encoder and image decoder, to achieve higher compression ratios and accelerated performance. We may also extend PTQD to a wider range of generative tasks to assess its efficacy and generalizability.

Limitations and Broader Impacts. The proposed PTQD framework stands out for its high efficiency and energy-saving properties, which carry significant implications in reducing the carbon emissions attributed to the widespread deployment of diffusion models. However, similar to other deep generative models, PTQD has the potential to be utilized for producing counterfeit images and videos for malicious purposes.

Acknowledgement This work was supported by National Key Research and Development Program of China (2022YFC3602601).

References

- [1] F. Bao, C. Li, J. Sun, J. Zhu, and B. Zhang. Estimating the optimal covariance with imperfect mean in diffusion probabilistic models. In *ICML*, 2022.
- [2] F. Bao, C. Li, J. Zhu, and B. Zhang. Analytic-dpm: an analytic estimate of the optimal reverse variance in diffusion probabilistic models. In *ICLR*, 2022.
- [3] N. D. Blog. Int4 for ai inference. <https://developer.nvidia.com/blog/int4-for-ai-inference/>, May 2021. Accessed on: May 1, 2023.
- [4] Y. Cai, Z. Yao, Z. Dong, A. Gholami, M. W. Mahoney, and K. Keutzer. Zeroq: A novel zero shot quantization framework. In *CVPR*, 2020.
- [5] N. Chen, Y. Zhang, H. Zen, R. J. Weiss, M. Norouzi, and W. Chan. Wavegrad: Estimating gradients for waveform generation. In *ICLR*, 2021.
- [6] W. Chen, P. Wang, and J. Cheng. Towards mixed-precision quantization of neural networks via constrained optimization. In *ICCV*, 2021.
- [7] H. Chung, B. Sim, and J. C. Ye. Come-closer-diffuse-faster: Accelerating conditional diffusion models for inverse problems through stochastic contraction. In *CVPR*, 2022.
- [8] H. Chung and J. C. Ye. Score-based diffusion models for accelerated mri. *Medical Image Analysis*, 80:102479, 2022.
- [9] R. D’AGOSTINO and E. S. Pearson. Tests for departure from normality. empirical results for the distributions of b^2 and \sqrt{b} . *Biometrika*, 60(3):613–622, 1973.
- [10] J. Deng, W. Dong, R. Socher, L.-J. Li, K. Li, and L. Fei-Fei. Imagenet: A large-scale hierarchical image database. In *CVPR*, 2009.
- [11] P. Dhariwal and A. Q. Nichol. Diffusion models beat gans on image synthesis. In *NeurIPS*, pages 8780–8794, 2021.
- [12] R. DIAgostino. An omnibus test of normality for moderate and large sample sizes. *Biometrika*, 58(34):1–348, 1971.
- [13] Z. Dong, Z. Yao, A. Gholami, M. W. Mahoney, and K. Keutzer. Hawq: Hessian aware quantization of neural networks with mixed-precision. In *ICCV*, 2019.
- [14] G. Franzese, S. Rossi, L. Yang, A. Finamore, D. Rossi, M. Filippone, and P. Michiardi. How much is enough? a study on diffusion times in score-based generative models. *arXiv preprint arXiv:2206.05173*, 2022.
- [15] G. Giannone, D. Nielsen, and O. Winther. Few-shot diffusion models. *arXiv preprint arXiv:2205.15463*, 2022.
- [16] R. Gong, X. Liu, S. Jiang, T. Li, P. Hu, J. Lin, F. Yu, and J. Yan. Differentiable soft quantization: Bridging full-precision and low-bit neural networks. In *ICCV*, 2019.
- [17] I. Goodfellow, J. Pouget-Abadie, M. Mirza, B. Xu, D. Warde-Farley, S. Ozair, A. Courville, and Y. Bengio. Generative adversarial networks. *Communications of the ACM*, 63(11):139–144, 2020.
- [18] M. Heusel, H. Ramsauer, T. Unterthiner, B. Nessler, and S. Hochreiter. Gans trained by a two time-scale update rule converge to a local nash equilibrium. In *NeurIPS*, volume 30, 2017.
- [19] J. Ho, A. Jain, and P. Abbeel. Denoising diffusion probabilistic models. In *NeurIPS*, 2020.
- [20] J. Ho, T. Salimans, A. A. Gritsenko, W. Chan, M. Norouzi, and D. J. Fleet. Video diffusion models. In *NeurIPS*, 2022.
- [21] X. Huang, Z. Shen, S. Li, Z. Liu, H. Xianghong, J. Wicaksana, E. Xing, and K.-T. Cheng. Sdq: Stochastic differentiable quantization with mixed precision. In *ICML*, 2022.
- [22] I. Hubara, Y. Nahshan, Y. Hanani, R. Banner, and D. Soudry. Improving post training neural quantization: Layer-wise calibration and integer programming. *arXiv preprint arXiv:2006.10518*, 2020.
- [23] B. Jacob, S. Kligys, B. Chen, M. Zhu, M. Tang, A. Howard, H. Adam, and D. Kalenichenko. Quantization and training of neural networks for efficient integer-arithmetic-only inference. In *CVPR*, 2018.
- [24] B. Jacob, S. Kligys, B. Chen, M. Zhu, M. Tang, A. Howard, H. Adam, and D. Kalenichenko. Quantization and training of neural networks for efficient integer-arithmetic-only inference. In *CVPR*, 2018.
- [25] A. Jolicoeur-Martineau, K. Li, R. Piché-Taillefer, T. Kachman, and I. Mitliagkas. Gotta go fast when generating data with score-based models. *arXiv preprint arXiv:2105.14080*, 2021.
- [26] T. Karras, M. Aittala, T. Aila, and S. Laine. Elucidating the design space of diffusion-based generative models. In *NeurIPS*, 2022.

- [27] A. Kerr, D. Merrill, J. Demouth, and J. Tran. Cutlass: Fast linear algebra in cuda c++. *NVIDIA Developer Blog*, 2017.
- [28] B. Kim and J. C. Ye. Denoising mcmc for accelerating diffusion-based generative models. In *ICML*, 2023.
- [29] D. Kingma, T. Salimans, B. Poole, and J. Ho. Variational diffusion models. In *NeurIPS*, 2021.
- [30] D. P. Kingma and M. Welling. Auto-encoding variational bayes. In *ICLR*, 2014.
- [31] Z. Kong and W. Ping. On fast sampling of diffusion probabilistic models. In *ICLR*, 2023.
- [32] M. W. Y. Lam, J. Wang, D. Su, and D. Yu. BDDM: bilateral denoising diffusion models for fast and high-quality speech synthesis. In *ICLR*, 2022.
- [33] A. Levkovitch, E. Nachmani, and L. Wolf. Zero-shot voice conditioning for denoising diffusion TTS models. In *Interspeech*, pages 2983–2987, 2022.
- [34] X. Li, Y. Liu, L. Lian, H. Yang, Z. Dong, D. Kang, S. Zhang, and K. Keutzer. Q-diffusion: Quantizing diffusion models. In *ICCV*, 2023.
- [35] Y. Li, R. Gong, X. Tan, Y. Yang, P. Hu, Q. Zhang, F. Yu, W. Wang, and S. Gu. BRECQ: pushing the limit of post-training quantization by block reconstruction. In *ICLR*, 2021.
- [36] Y. Lin, T. Zhang, P. Sun, Z. Li, and S. Zhou. Fq-vit: Post-training quantization for fully quantized vision transformer. In *IJCAI*, 2022.
- [37] L. Liu, Y. Ren, Z. Lin, and Z. Zhao. Pseudo numerical methods for diffusion models on manifolds. In *ICLR*, 2022.
- [38] C. Louizos, M. Reisser, T. Blankevoort, E. Gavves, and M. Welling. Relaxed quantization for discretized neural networks. In *ICLR*, 2019.
- [39] C. Lu, Y. Zhou, F. Bao, J. Chen, C. Li, and J. Zhu. Dpm-solver: A fast ODE solver for diffusion probabilistic model sampling in around 10 steps. In *NeurIPS*, 2022.
- [40] C. Lu, Y. Zhou, F. Bao, J. Chen, C. Li, and J. Zhu. Dpm-solver++: Fast solver for guided sampling of diffusion probabilistic models. *arXiv preprint arXiv:2211.01095*, 2022.
- [41] E. Luhman and T. Luhman. Knowledge distillation in iterative generative models for improved sampling speed. *arXiv preprint arXiv:2101.02388*, 2021.
- [42] S. Luo and W. Hu. Diffusion probabilistic models for 3d point cloud generation. In *CVPR*, 2021.
- [43] Z. Lyu, X. Xu, C. Yang, D. Lin, and B. Dai. Accelerating diffusion models via early stop of the diffusion process. *arXiv preprint arXiv:2205.12524*, 2022.
- [44] M. Nagel, R. A. Amjad, M. van Baalen, C. Louizos, and T. Blankevoort. Up or down? adaptive rounding for post-training quantization. In *ICML*, volume 119, pages 7197–7206, 2020.
- [45] M. Nagel, M. van Baalen, T. Blankevoort, and M. Welling. Data-free quantization through weight equalization and bias correction. In *ICCV*, pages 1325–1334, 2019.
- [46] C. Nash, J. Menick, S. Dieleman, and P. W. Battaglia. Generating images with sparse representations. In *ICML*, volume 139, pages 7958–7968, 2021.
- [47] A. Q. Nichol and P. Dhariwal. Improved denoising diffusion probabilistic models. In *ICML*, 2021.
- [48] NVIDIA Corporation. TensorRT. <https://developer.nvidia.com/tensorrt>, 2019. [Online; accessed 30 April 2023].
- [49] R. Rombach, A. Blattmann, D. Lorenz, P. Esser, and B. Ommer. High-resolution image synthesis with latent diffusion models. In *CVPR*, pages 10674–10685, 2022.
- [50] T. Salimans, I. Goodfellow, W. Zaremba, V. Cheung, A. Radford, and X. Chen. Improved techniques for training gans. In *NeurIPS*, volume 29, 2016.
- [51] T. Salimans and J. Ho. Progressive distillation for fast sampling of diffusion models. In *ICLR*, 2022.
- [52] Y. Shang, Z. Yuan, B. Xie, B. Wu, and Y. Yan. Post-training quantization on diffusion models. *arXiv preprint arXiv:2211.15736*, 2022.
- [53] C. Shi, S. Luo, M. Xu, and J. Tang. Learning gradient fields for molecular conformation generation. In *ICML*, 2021.
- [54] J. Song, C. Meng, and S. Ermon. Denoising diffusion implicit models. In *ICLR*, 2021.
- [55] Y. Song, J. Sohl-Dickstein, D. P. Kingma, A. Kumar, S. Ermon, and B. Poole. Score-based generative modeling through stochastic differential equations. In *ICLR*, 2021.
- [56] P. Virtanen, R. Gommers, T. E. Oliphant, M. Haberland, T. Reddy, D. Cournapeau, E. Burovski, P. Peterson, W. Weckesser, J. Bright, et al. Scipy 1.0: fundamental algorithms for scientific computing in python. *Nature methods*, 17(3):261–272, 2020.

- [57] V. Voleti, A. Jolicoeur-Martineau, and C. Pal. MCVD - masked conditional video diffusion for prediction, generation, and interpolation. In *NeurIPS*, 2022.
- [58] P. Wang, Q. Chen, X. He, and J. Cheng. Towards accurate post-training network quantization via bit-split and stitching. In *ICML*, 2020.
- [59] Y. Wang, Y. Lu, and T. Blankevoort. Differentiable joint pruning and quantization for hardware efficiency. In *ECCV*, 2020.
- [60] D. Watson, W. Chan, J. Ho, and M. Norouzi. Learning fast samplers for diffusion models by differentiating through sample quality. In *ICLR*, 2022.
- [61] D. Watson, J. Ho, M. Norouzi, and W. Chan. Learning to efficiently sample from diffusion probabilistic models. *arXiv preprint arXiv:2106.03802*, 2021.
- [62] X. Wei, R. Gong, Y. Li, X. Liu, and F. Yu. Qdrop: Randomly dropping quantization for extremely low-bit post-training quantization. In *ICLR*, 2022.
- [63] W. Wu, Y. Zhao, M. Z. Shou, H. Zhou, and C. Shen. Diffumask: Synthesizing images with pixel-level annotations for semantic segmentation using diffusion models. *arXiv preprint arXiv:2303.11681*, 2023.
- [64] H. Yang, L. Duan, Y. Chen, and H. Li. BSQ: exploring bit-level sparsity for mixed-precision neural network quantization. In *ICLR*, 2021.
- [65] F. Yu, A. Seff, Y. Zhang, S. Song, T. Funkhouser, and J. Xiao. Lsun: Construction of a large-scale image dataset using deep learning with humans in the loop. *arXiv preprint arXiv:1506.03365*, 2015.
- [66] L. Zhang, Y. He, Z. Lou, X. Ye, Y. Wang, and H. Zhou. Root quantization: a self-adaptive supplement ste. *Applied Intelligence*, 53(6):6266–6275, 2023.
- [67] Q. Zhang and Y. Chen. Fast sampling of diffusion models with exponential integrator. *arXiv preprint arXiv:2204.13902*, 2022.
- [68] Q. Zhang, M. Tao, and Y. Chen. gddim: Generalized denoising diffusion implicit models. In *ICLR*, 2023.
- [69] H. Zheng, P. He, W. Chen, and M. Zhou. Truncated diffusion probabilistic models. *stat*, 1050:7, 2022.
- [70] B. Zhuang, C. Shen, M. Tan, L. Liu, and I. Reid. Towards effective low-bitwidth convolutional neural networks. In *CVPR*, 2018.

Appendix

We organize our supplementary material as follows:

- In section **A**, we provide a comprehensive explanation of extending PTQD to DDIM [54].
- In section **B**, we show the statistical analysis of quantization noise.
- In section **C**, we present additional experimental results.
- In section **D**, we provide additional visualization results on ImageNet and LSUN dataset.

A Extending PTQD to DDIM

DDIM [54] generalizes DDPMs [19] via a class of non-Markovian diffusion processes, which can greatly accelerate the sampling process. Briefly, when DDIM is quantized, the sampling of \mathbf{x}_{t-1} can be expressed as:

$$\begin{aligned}\mathbf{x}_{t-1} &= \sqrt{\alpha_{t-1}} \left(\frac{\mathbf{x}_t - \sqrt{1 - \alpha_t} \hat{\epsilon}_\theta(\mathbf{x}_t, t)}{\sqrt{\alpha_t}} \right) + \sqrt{1 - \alpha_{t-1} - \sigma_t^2} \hat{\epsilon}_\theta(\mathbf{x}_t, t) + \sigma_t \mathbf{z} \\ &= \sqrt{\alpha_{t-1}} \left(\frac{\mathbf{x}_t - \sqrt{1 - \alpha_t} (\epsilon_\theta(\mathbf{x}_t, t) + \Delta_{\epsilon_\theta(\mathbf{x}_t, t)})}{\sqrt{\alpha_t}} \right) + \sqrt{1 - \alpha_{t-1} - \sigma_t^2} (\epsilon_\theta(\mathbf{x}_t, t) + \Delta_{\epsilon_\theta(\mathbf{x}_t, t)}) + \sigma_t \mathbf{z}\end{aligned}\quad (\text{A})$$

where $\hat{\epsilon}_\theta(\mathbf{x}_t, t)$ is the result of quantized noise prediction network and $\Delta_{\epsilon_\theta(\mathbf{x}_t, t)}$ is the quantization noise.

Firstly, we disentangle the quantization noise to its correlated and residual uncorrelated part, which is same as in DDPM [19]:

$$\Delta_{\epsilon_\theta(\mathbf{x}_t, t)} = k \epsilon_\theta(\mathbf{x}_t, t) + \Delta'_{\epsilon_\theta(\mathbf{x}_t, t)}. \quad (\text{B})$$

Then we can reformulate Eq. (A) as

$$\begin{aligned}\mathbf{x}_{t-1} &= \sqrt{\alpha_{t-1}} \left(\frac{\mathbf{x}_t - \sqrt{1 - \alpha_t} \left((1+k) \epsilon_\theta(\mathbf{x}_t, t) + \Delta'_{\epsilon_\theta(\mathbf{x}_t, t)} \right)}{\sqrt{\alpha_t}} \right) \\ &\quad + \sqrt{1 - \alpha_{t-1} - \sigma_t^2} \left((1+k) \epsilon_\theta(\mathbf{x}_t, t) + \Delta'_{\epsilon_\theta(\mathbf{x}_t, t)} \right) + \sigma_t \mathbf{z}.\end{aligned}\quad (\text{C})$$

By estimating the correlation coefficient k , the correlated part can be corrected by dividing the output of the quantized noise prediction network $\hat{\epsilon}_\theta(\mathbf{x}_t, t)$ by $1+k$:

$$\begin{aligned}\mathbf{x}_{t-1} &= \sqrt{\alpha_{t-1}} \left(\frac{\mathbf{x}_t - \sqrt{1 - \alpha_t} \epsilon_\theta(\mathbf{x}_t, t)}{\sqrt{\alpha_t}} \right) + \sqrt{1 - \alpha_{t-1} - \sigma_t^2} \epsilon_\theta(\mathbf{x}_t, t) \\ &\quad + \left(\frac{\sqrt{1 - \alpha_{t-1} - \sigma_t^2}}{1+k} - \frac{\sqrt{\alpha_{t-1}} \sqrt{1 - \alpha_t}}{(1+k) \sqrt{\alpha_t}} \right) \Delta'_{\epsilon_\theta(\mathbf{x}_t, t)} + \sigma_t \mathbf{z}.\end{aligned}\quad (\text{D})$$

Then we calibrate the variance schedule, denoted as σ_t' , to absorb the excess variance of residual quantization noise, which is depicted by σ_q^2 . Let $\lambda_t = \frac{\sqrt{1 - \alpha_{t-1} - \sigma_t^2}}{1+k} - \frac{\sqrt{\alpha_{t-1}} \sqrt{1 - \alpha_t}}{(1+k) \sqrt{\alpha_t}}$, we have:

$$\lambda_t^2 \sigma_q^2 + \sigma_t'^2 = \sigma_t^2, \quad (\text{E})$$

$$\sigma_t'^2 = \begin{cases} \sigma_t^2 - \lambda_t^2 \sigma_q^2, & \text{if } \sigma_t^2 \geq \lambda_t^2 \sigma_q^2 \\ 0, & \text{otherwise.} \end{cases} \quad (\text{F})$$

B Statistical analysis

Distribution of residual quantization noise. We first perform statistical tests to verify if the residual quantization noise adheres to a Gaussian distribution. To accomplish this, we employ the significance test *scipy.stats.normaltest* provided by Scipy [56]. This test is based on D'Agostino and Pearson's

test [12, 9], with the null hypothesis proposing that the sample comes from a normal distribution. The outcomes are illustrated in Figure A, and they reveal that, with a significance level of 0.01, the null hypothesis cannot be rejected at any step, thus substantiating our assumption. In Figure B, we present the variance of the residual uncorrelated quantization noise. It can be observed that as the quantization bitwidth decreases, the variance of the quantization noise increases accordingly. Nonetheless, the coefficient associated with this variance is relatively small, allowing for its effective absorption into the calibrated diffusion variance schedule. Figure C illustrates the bias on the estimated mean introduced by the residual quantization noise. Notably, this bias exhibits significant variations across different channels, emphasizing the necessity for distinct correction procedures for each channel.

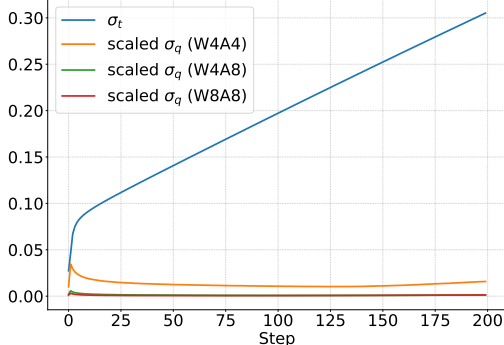
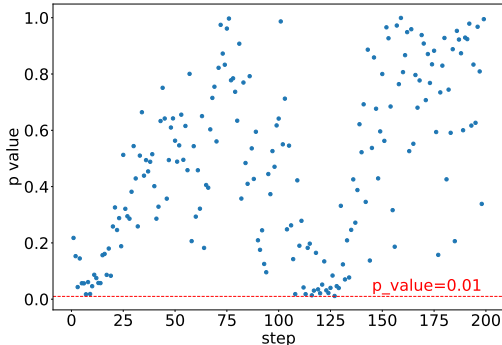


Figure A: The result of normal test for residual quantization noise across various steps. Data is collected from W4A4 LDM-8 on LSUN-Churches.

Figure B: Comparison of the variance schedule and the scaled variance of quantization noise from LDM-4 on LSUN-Churches. Here, the scale for σ_q refers to the coefficient in Eq. (12) in the paper.

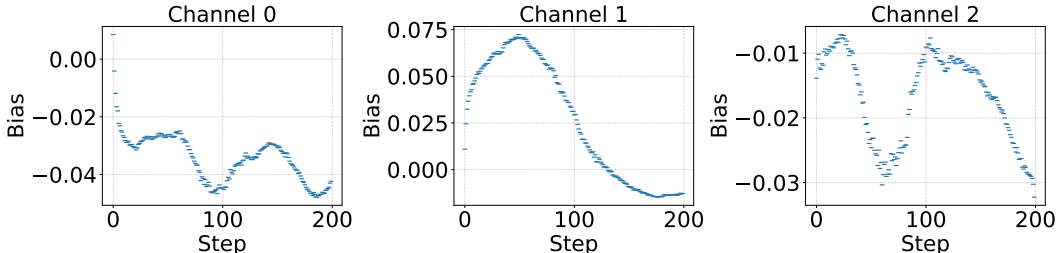


Figure C: Channel-wise bias of residual quantization noise. Data is collected from W4A4 LDM-8 on LSUN-Churches.

Correlation analysis. In Figures D to G, we present the results of linear regression analysis conducted on the quantization noise and the output of the full-precision noise estimation network, which includes Pearson’s coefficient R and the coefficient k as defined in Eq. (B). As depicted in Figures E and G, we observe a notably high R value for diffusion models with W4A4 bitwidth, indicating that the quantization noise primarily consists of the correlated component. This finding demonstrates the effectiveness of our method in rectifying this specific aspect of quantization noise, particularly in scenarios involving low bitwidth. In cases of diffusion models with W4A8 or W8A8 bitwidth, our approach can also correct a substantial portion of the quantization noise by leveraging the correlation. Additionally, for larger steps, the coefficient k generally exhibits positive values (which can also be observed in Figures E and G, as k and R value share the same sign), thereby affirming our capability to correct the correlated part of the quantization noise in these steps.

C Additional experimental results

C.1 Implementation details of step-aware mixed precision

Table E presents the results of bitwidth allocation for each dataset, which are determined by Eq. (15) in the paper.

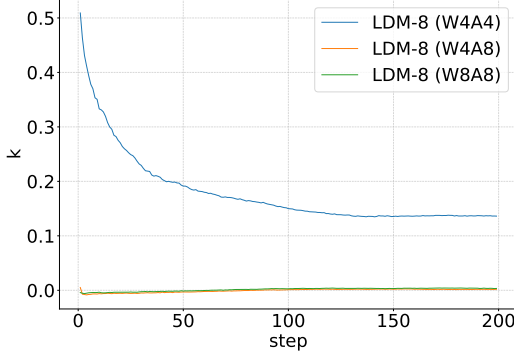


Figure D: The correlation coefficient k in each step of LDM-8 on LSUN-Churches.

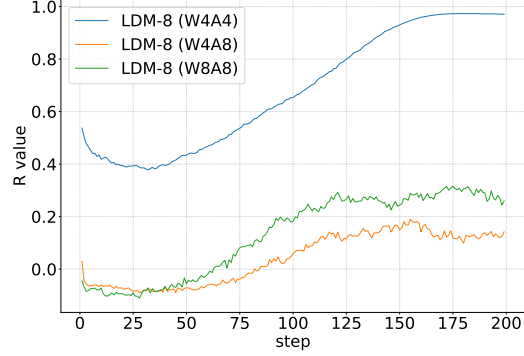


Figure E: The R value of linear regression in each step of LDM-8 on LSUN-Churches.

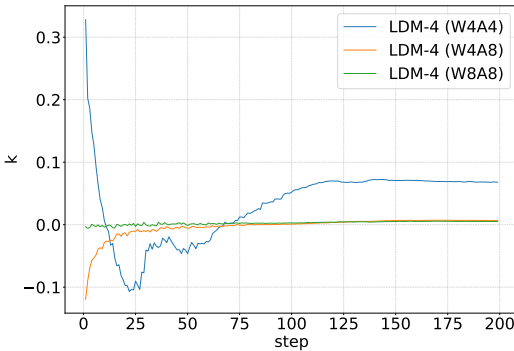


Figure F: The correlation coefficient k in each step of LDM-4 on LSUN-Bedrooms.

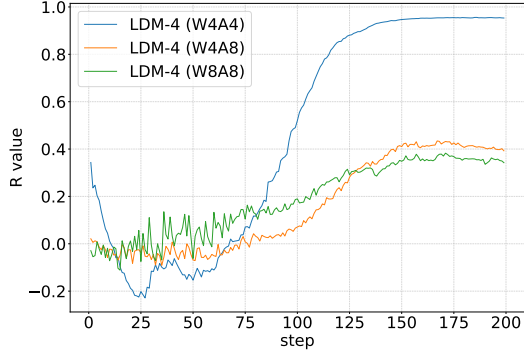


Figure G: The R value of linear regression in each step of LDM-4 on LSUN-Bedrooms.

C.2 Additional ablation experiments

In this section, we conduct additional ablation experiments with constant precision, which are outlined in Table F. The experimental results consistently demonstrate performance improvements brought by each component of our method under constant precision settings. Notably, our method exhibits more significant improvements at lower bitwidth (W3A8) due to the inherent presence of greater quantization noise at these levels.

C.3 Comparisons with PTQ4DM

Additionally, we include a comparison with the PTQ method PTQ4DM [52] on the LSUN-Bedrooms dataset, as shown in Table G. Remarkably, our proposed approach outperforms PTQ4DM in both W4A8 and W3A8 bitwidth scenarios.

C.4 Evaluation with advanced sampler

Table H presents the results on a new dataset CelebA-HQ over recent DDPM variants PLMS [37], demonstrating the strong performance of PTQD under this configuration. Notably, the proposed PTQD reduces the FID and sFID by a considerable margin of 3.23 and 4.73 in comparison to Q-Diffusion, respectively.

Additionally, we present the results of our PTQD over latest DPM++ solver [40] on LSUN-Churches dataset, as shown in Table I. Notably, our PTQD with W3A8 bitwidth achieves a sFID result comparable to that of W4A8 Q-Diffusion.

Table E: Bitwidth allocation for each dataset.

Dataset	W4A4 Step Range	W4A8 Step Range
ImageNet (250 steps)	249 to 202	201 to 0
ImageNet (20 steps)	19 to 15	14 to 0
LSUN-Bedrooms	199 to 155	154 to 0
LSUN-Churches	199 to 146	145 to 0

Table F: Additional ablation study with constant precision on LSUN-Bedrooms dataset. As the bitwidth decreases, the efficacy of our approach becomes increasingly pronounced.

Model	Method	Bitwidth (W/A)	FID↓	sFID↓
	FP	32/32	3.00	7.13
	Q-Diffusion	4/8	6.72	18.80
	+CNC	4/8	6.31	16.28
	+CNC+VSC	4/8	6.10	16.03
LDM-4 (steps=200 eta=1.0)	PTQD (CNC+VSC+BC)	4/8	5.94	15.16
	Q-Diffusion	3/8	8.31	21.06
	+CNC	3/8	7.01	18.32
	+CNC+VSC	3/8	6.66	17.99
	PTQD (CNC+VSC+BC)	3/8	6.46	17.04

C.5 Evaluation with different variance schedule

Table J presents experimental results with deterministic and stochastic sampling on FFHQ and ImageNet dataset over LDM-4 model. While deterministic sampling has gained widespread adoption, it tends to result in lower output quality compared to stochastic sampling [55, 26]. Specifically, when generating samples on FFHQ dataset with a deterministic DDIM sampler, introducing stochastic perturbations lower both the FID and sFID metrics. For experiments on ImageNet dataset, it greatly improves the IS with little increase in FID and sFID.

Table G: Performance comparisons with PTQ4DM on LSUN-Bedrooms dataset over LDM-4 model.

Model	Method	Bitwidth (W/A)	FID↓	sFID↓
LDM-4 (steps=200 eta=1.0)	FP	32/32	3.00	7.13
	PTQ4DM	4/8	20.72	54.30
	Q-Diffusion	4/8	6.72	18.80
	Ours	4/8	5.94	15.16
	PTQ4DM	3/8	22.17	51.93
	Q-Diffusion	3/8	8.31	21.06
	Ours	3/8	6.46	17.04

Table H: Experimental results on CelebA-HQ dataset with PLMS sampler.

Model	Method	Bitwidth (W/A)	FID↓	sFID↓
LDM-4 (steps=200 eta=0.0)	FP	32/32	16.72	15.97
	Q-Diffusion	4/8	24.31	22.11
	Ours	4/8	21.08	17.38

Table I: Experimental results on LSUN-Churches dataset with DPM++ sampler.

Model	Method	Bitwidth (W/A)	FID	sFID
LDM-8 (steps = 50 eta = 0.0)	FP	32/32	5.97	21.50
	Q-Diffusion	4/8	7.80	23.24
	Ours	4/8	7.45	22.74
	Q-Diffusion	3/8	11.44	24.67
	Ours	3/8	10.72	23.36

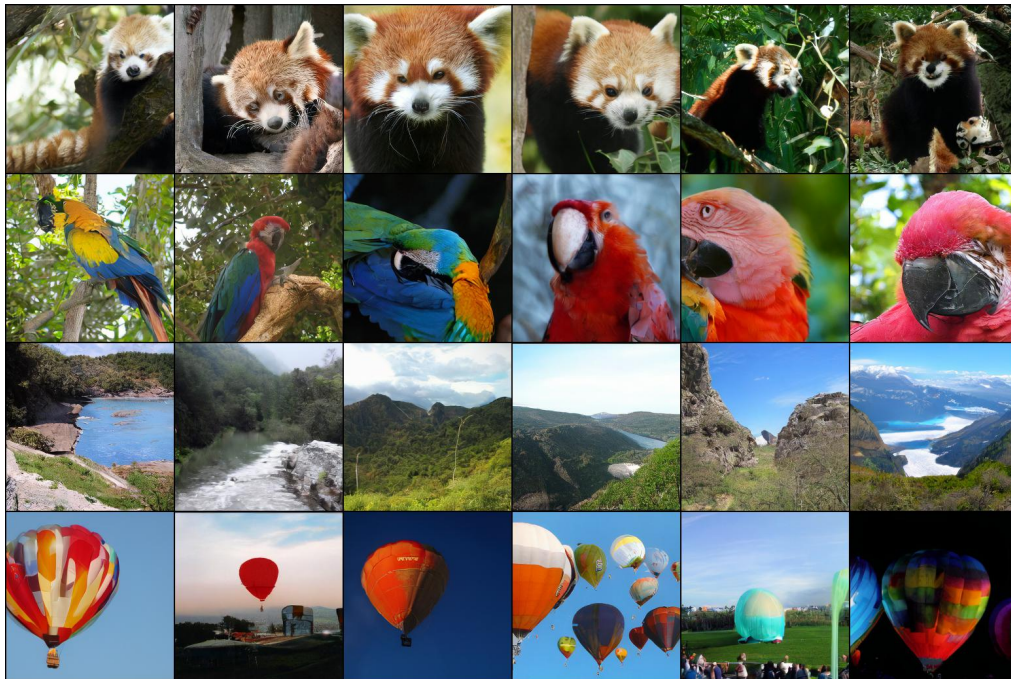
Table J: Comparisons of generated sample quality under different variance schedules (denoted by *eta* below).

Model	Dataset	<i>eta</i>	IS↑	FID↓	sFID↓
LDM-4 (steps=200)	FFHQ	0.0	-	11.26	8.36
		1.0	-	9.37	7.04
LDM-4 (steps=250)	ImageNet	0.0	150.04	4.35	6.20
		1.0	185.04	5.05	7.10

D Additional visualization results



(a) samples generated with 20 steps



(b) samples generated with 250 steps

Figure H: Class-conditional generation on ImageNet 256×256 . With the proposed PTQD, LDM-4 [49] with W4A8 bitwidth can generate high-fidelity images in only 20 steps.

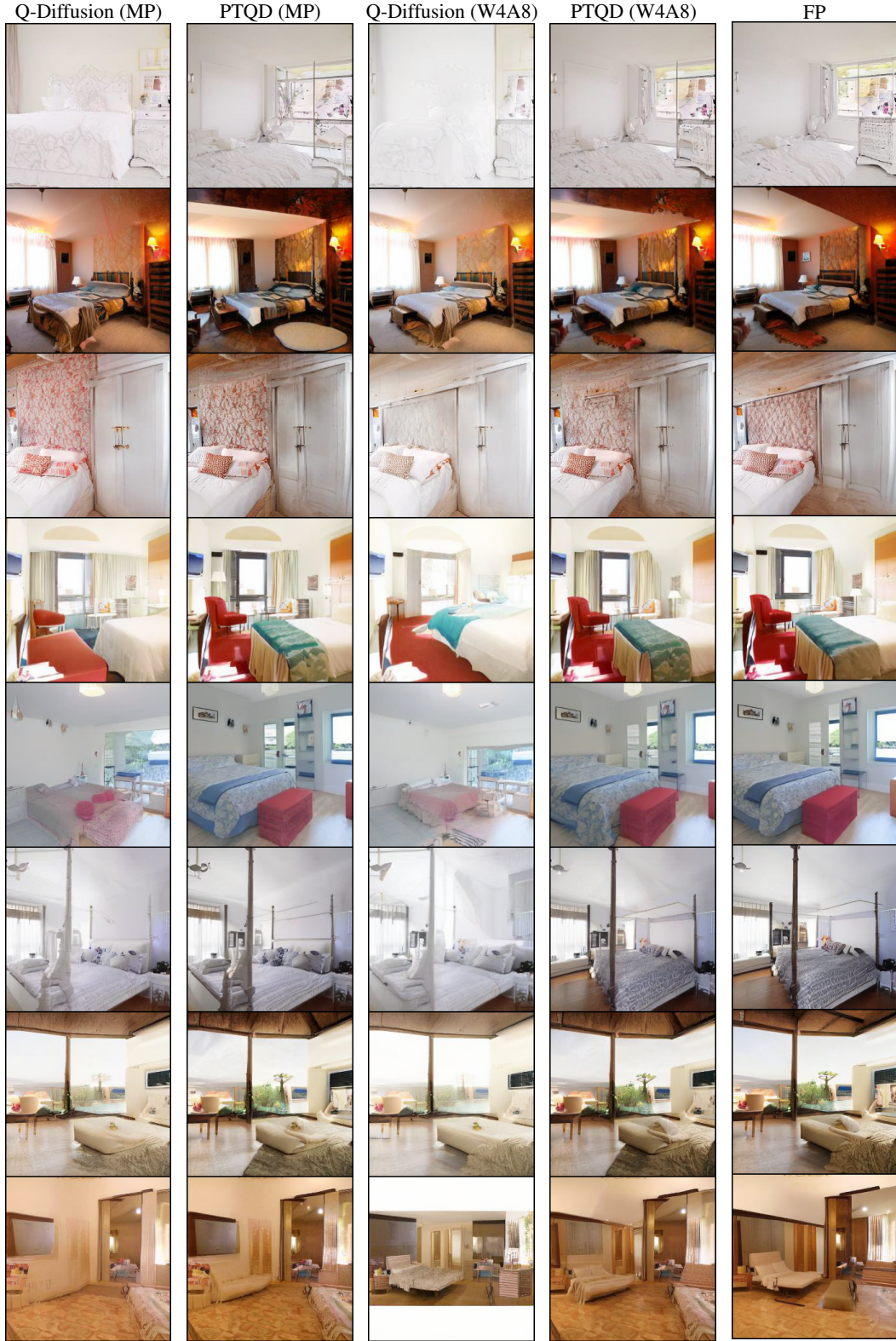


Figure I: The comparisons of samples generated by Q-Diffusion [34], PTQD and full-precision LDM-4 [49] on LSUN-Bedrooms 256×256 . Compared with Q-Diffusion, samples generated by PTQD are less affected by quantization noise and exhibit a closer resemblance to the results of the full-precision model.

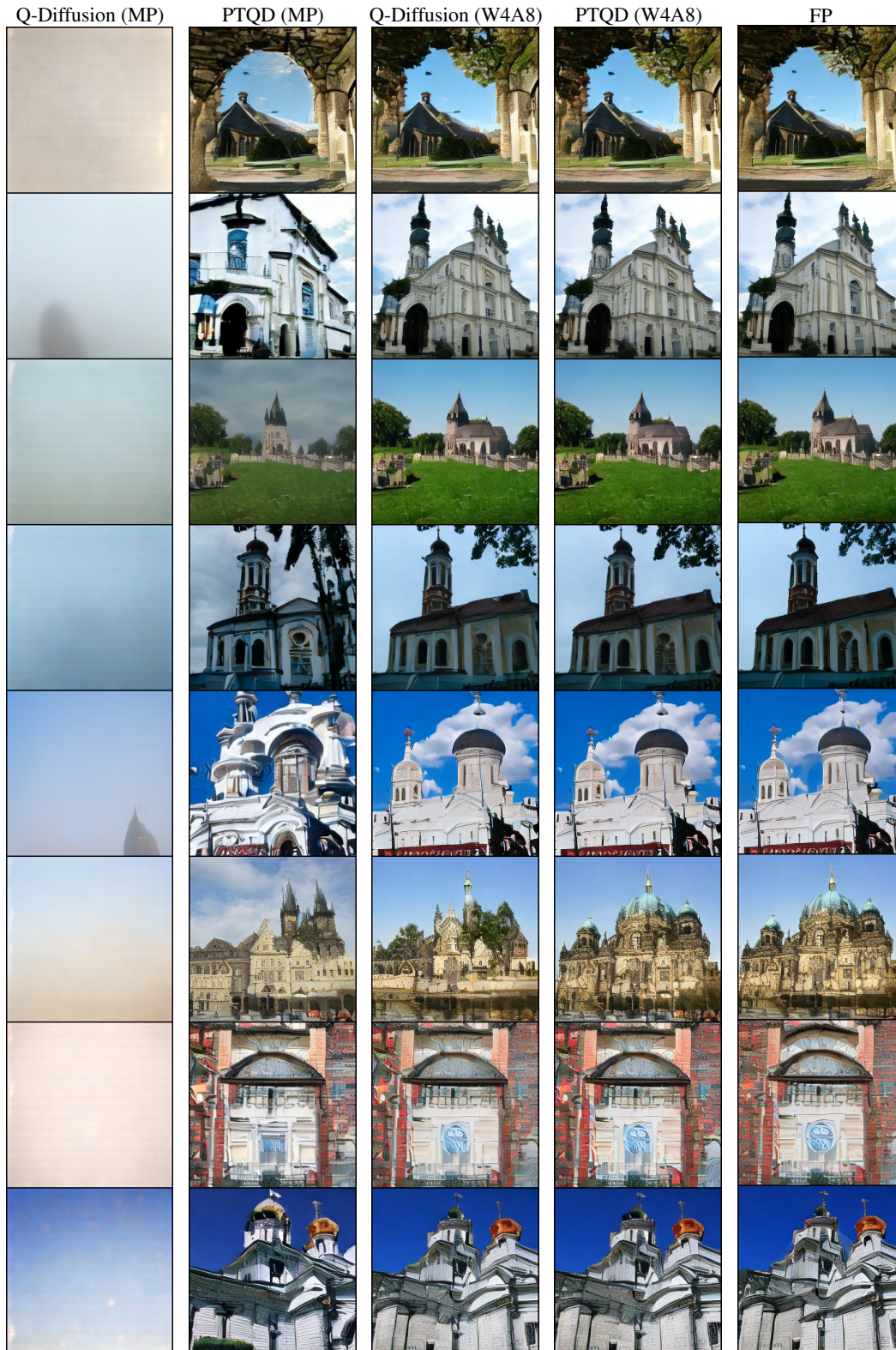


Figure J: The comparisons of samples generated by Q-Diffusion [34], PTQD and full-precision LDM-8 [49] on LSUN-Churches 256×256 . While Q-Diffusion fails to denoise when utilizing W4A4 model in the mixed precision setting, PTQD, on the other hand, can still generate high-quality images under these conditions.